FOI-R--0146--SE

June 2001

ISSN 1650-1942

Technical report

Eva Dalberg

A Measurement of the Underwater Electric Field Off the West Coast of Sweden

Issuing organization	Report number, ISRN	Report type
FOI – Swedish Defence Research Agency Systems Technology SE-172 90 Stockholm	FOI-R--0146--SE	Technical report
	Research area code 4. C4ISR	
	Month year June 2001	**Project no.** E6008
	Customers code 5. Contracted Research	
	Sub area code 43 Underwater Surveillance Sensors	

Author/s (editor/s)	Project manager
Eva Dalberg	Johan Mattsson
	Approved by
	Scientifically and technically responsible Peter Sigray

Report title

A Measurement of the Underwater Electric Field Off the West Coast of Sweden

Abstract (not more than 200 words)

The underwater electric field has been measured during a 10-month period by two three-axis electrode systems in shallow water off the west coast of Sweden. The long-term performance of the systems has been evaluated. One out of the six channels failed at the end of the experimental period.

Data were collected in 10-minute intervals, at most once per hour. The measurement covers frequencies from a few mHz up to 20 Hz. The natural background in this frequency interval has been characterized. It contains sources of various origins, where man-made sources dominate at the higher frequencies. At lower frequencies micropulsations are important.

The two systems were separated by approximately 720 m. The correlation between the signals in the two systems is high, which implies that non-local sources constitute the main part of the received signal. One system may thus be used for reference filtering, where a large part of the background can be removed.

Keywords

ELFE background; ULF band; underwater; long-term measurement; electric field

Further bibliographic information	Language English
ISSN 1650-1942	**Pages** 27 p.
	Price acc. to pricelist **Security classification**

Utgivare	Rapportnummer, ISRN	Klassificering
Totalförsvarets Forskningsinstitut - FOI Systemteknik 172 90 Stockholm	FOI-R--0146--SE	Teknisk rapport
	Forskningsområde 4. Spaning och ledning	
	Månad, år Juni 2001	**Projektnummer** E6008
	Verksamhetsgren 5. Uppdragsfinansierad verksamhet	
	Delområde 43 Undervattenssensorer	
Författare/redaktör Eva Dalberg	**Projektledare** Johan Mattsson	
	Godkänd av	
	Tekniskt och/eller vetenskapligt ansvarig Peter Sigray	

Rapportens titel (i översättning)

En mätning av det elektriska fältet i vatten utanför den svenska västkusten

Sammanfattning (högst 200 ord)

Under en 10-månaders period har det elektriska fältet mätts med två stycken tre-axliga elektrodsystem i grunt vatten vid den svenska västkusten. Systemens prestanda under denna tidsrymd har utvärderats. En av de sex mätkanalerna slutade att fungera i slutfasen av mätperioden.

Data samlades in i 10-minuters perioder, som mest varje timme. Mätningarna omfattade frekvenser från några mHz upp til 20 Hz. Den naturliga bakgrunden i detta frekvensområde har undersökts. Denna bakgrund har många olika typer av källor. Vid de högre frekvenserna dominerar brus orsakat av mänskliga aktiviteter. Vid lägre frekvenser är mikropulsationer viktiga.

Avståndet mellan de två systemen var cirka 720 m. Korrelationen mellan signaler mätta i de två systemen är hög, vilket betyder att källorna till fälten i första hand inte är av lokalt ursprung. Ett av systemen kan alltså användas som referenssystem vid så kallad referensfiltrering, och på så vis kan en stor del av bakgrunden elimineras.

Nyckelord

ELFE bakgrund; ULF band; undervatten; långtids mätning; electric field

Övriga bibliografiska uppgifter	Språk Engelska
ISSN 1650-1942	**Antal sidor:** 27 s.
Distribution enligt missiv	**Pris: Enligt prislista** **Sekretess**

1. Introduction

A long-term measurement with two separate electrode systems has been conducted off the west coast of Sweden. The analysed data were collected during a 10-month period. The primary aim was to investigate the performance of the systems in this environment over a longer period.

Electromagnetic underwater sensors in the form of electrodes, which are used to measure the electric field, utilize the conductivity of the seawater. The conductivity depends mainly on temperature and salinity. The potential between a pair of electrodes separated by some distance is measured. The electrode separation was between 2.4 m and 5 m in this experiment. Two types of electrodes were used, silver-silver chloride electrodes [1] in one of the systems and carbon fibre (graphite) electrodes [2] in the other.

It was also of interest to measure the natural electric field over a longer period. The underwater electric field has several origins. At lower frequencies, within the region of micropulsations (also called geomagnetic pulsations) in the ultra low frequency (ULF) band, the field can be rapidly changing over time. These pulsations are due to interactions in the Sun-Earth system that drives currents in the ionosphere and magnetosphere. At higher frequencies the Schumann resonances appear. They are caused by lightning activity that excite the Earth-ionosphere cavity at distinct frequencies. Noise from power-lines and other human activities can also affect the frequency spectrum covered by the measurement presented here. Occasional events may appear in the measured field due to the passage of a ship directly over the electrode system.

The two systems were deployed at approximately 720 m distance from each other. The correlation of the signal over this distance was also studied.

The site and the equipment used are described in Section 2. Section 3 concerns the long-term performance of the electrodes over the 10-month period covered by the measurements. Details on the evaluation methods are found in the appendices. The frequency content is further analysed in Section 4, and examples are given of the different types of signals. The correlation between the two systems is finally treated in Section 5.

2. The experiment

2.1. The site and the equipment

The site of the experiment is the Lysekil harbour, near the mouth of Gullmarsfjorden. To the west is Skagerack sea, outside a small archipelago. The harbour is commercial with freight traffic and there are some ferries with regular traffic in the area. Across the harbour is Lysekil town in near vicinity of the measurement site. A photo taken from the town of Lysekil towards the measurement site is shown in Figure 1.

Two systems were deployed. Their locations can be seen in Figure 2. The distance between the two positions A and B is approximately 720 m. System A is at a depth of 27 m, while System B, situated closer to the outflow of Gullmarsfjorden, is at the larger depth of 47 m. Table 1 summarize some of the key numbers of the two systems. Each system consists of three axes, one vertical and the other in the horizontal plane, orthogonal to each other. The alignment of the horizontal axes is nearly equal in the geomagnetic system for both electrode systems, with the x-axis approximately 55 degrees and the y-axis -35 degrees away from magnetic north. The crosses in Figure 2 indicate the positions of the systems. The labels used on the axes in this report is shown in this figure; z is pointing vertically down and the two horizontal axes are denoted by x and y respectively.

Figure 1: The measurement site. The photo was taken from the town of Lysekil westwards towards the measurement site. The mouth of Gullmarsfjorden is seen behind the crane in the centre. Skagerack Sea is to the right.

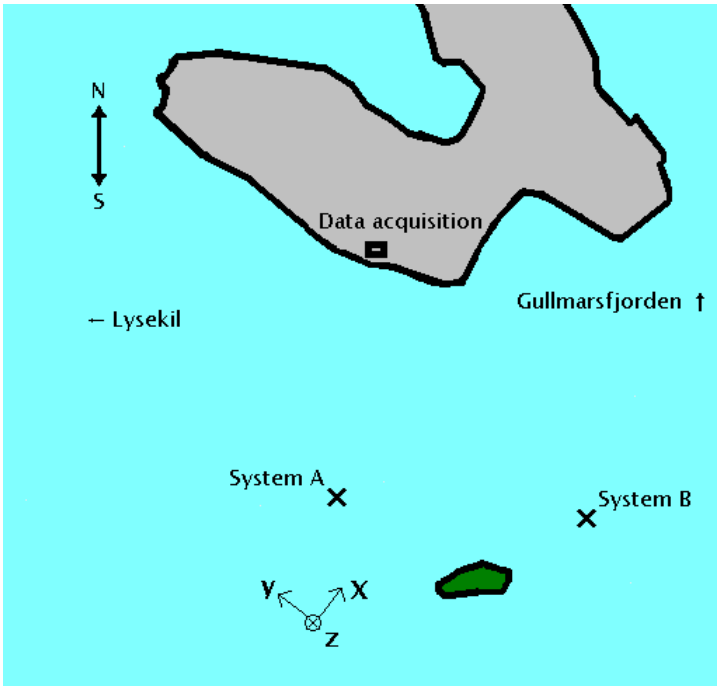

Figure 2: A schematic overview of the positions of the two electrode systems. The distance between the two systems is approximately 720 m. The data acquisition equipment is placed on land, nearby the harbour.

	System A, Ag/AgCl	*System B, C-fibre*
Position N	N58°16',138	N58°16',077
Position E	E11°27',014	E11°27',740
Depth	27 m	47 m
Alignment of x-axis versus magnetic north	54°	52°

Table 1: Key numbers of the two electrode systems.

Each axis is equipped with an electrode at each end. The distance between the two electrodes on the vertical axis is 2.4 m. The horizontal electrode pairs are separated by 5 m. The axes are made of plastic tubes (Davinyl PVC) and are mounted on a concrete foundation. Figure 3 shows the systems on land before deployment.

Each system has its own type of electrodes. System A, at shallow depth, is equipped with silver-silver chloride electrodes. The second system has carbon fibre electrodes. The former electrodes work in a conventional way. They are sensitive to an increased concentration of chloride ions in their neighbourhood through a chemical reaction that increases their surface potential [1]. The latter type is chemically inert, but responds to changes in the electric field through polarization of the electrode surface [2].

Cables from the electrodes are brought to shore where the data acquisition electronics is situated. Firstly, the signals are amplified 10000 times (by 80 dB) and low pass filtered at 10 Hz [3]. The potential difference between an electrode pair is connected to one data channel, which is digitized by a 23-bit analogue to digital converter. Theoretically the complete system is sensitive down to 0.02 nV/m, taking into account the number of bits in the analogue to digital converter, the amplification and the distance between the electrodes.

After digitization, data were sampled at a frequency of 40 Hz.

Figure 3: The two systems before deployment.

2.2. The data set

The data set analysed here covers the time between 29 June 2000 and 29 April 2001. Data were generally collected 10 minutes per hour, starting at 15 minutes past the hour, apart from a short period when there was 6 hours between the runs. There are gaps in the data set, due to various problems with the data acquisition system. Figure 4 shows the number of runs collected per week during the measurement period. In total 3286 10-minute runs have been analysed.

Even if there are gaps over time, the coverage over all weekdays and hours is more equal, which is shown in Figure 5. There is a tendency of decreased efficiency over weekends and at nights. This is because the system has to be restarted manually at the site. During the period with 6 hours between the runs, data were collected 15 minutes past the hours 3, 9, 15, and 21, which explains the peaks in the lower histogram in Figure 5.

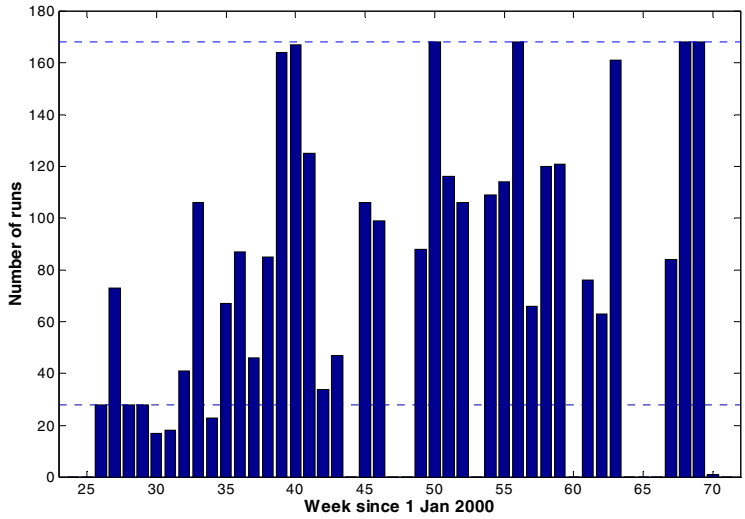

Figure 4: The number of analysed runs per week during the measurement period from 29 June 2000 to 29 April 2001. The upper dotted line shows the number of runs collected per week if there would be no gaps in the acquisition when the acquisition takes place hourly, and the lower dotted line when data is collected every 6 hours.

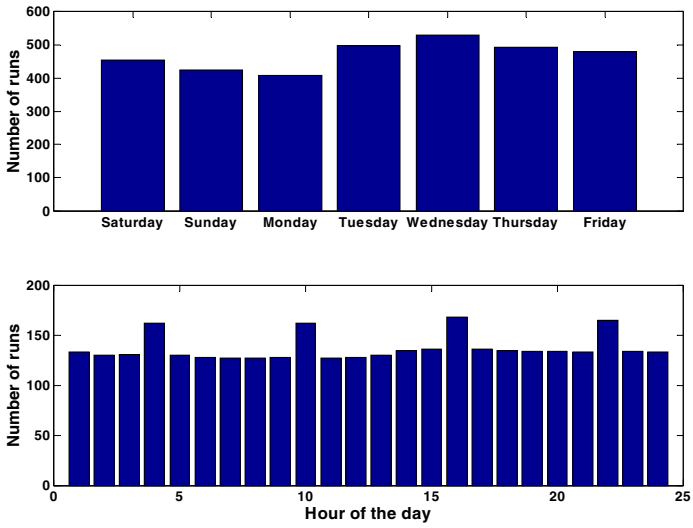

Figure 5: The number of runs analysed per weekday and per hour of the day. Data were collected every 6 hour for a period, which is the reason why there are peaks in the number of runs for some hours.

3. Long term performance of the electrodes

One of the aims of this study is to investigate the performance of the electrode systems in the environment at the site over a longer period. Figure 6 shows the time-series of the first 10 minutes of data used in the analysis, and the last 10 minutes are shown in Figure 7. The measured fields are a few μV/m in the beginning as well as in the end of the measurement period. The vertical components are smaller than the horizontal ones, as expected. This is because electric fields are damped in the direction perpendicular to a boundary between two layers with different conductivity, like air and water. Please note that the scale is different between the vertical and horizontal components, and for the z-component of system B in Figure 7, which shows data from the last run.

These two time-series are typical for their respective collection time. Looking at the time-series, the signals in the horizontal channels of both systems are very similar. That is true for data from the beginning as well as the end of the measurement period. Statistically the correlation between the horizontal channels is indeed very good, around 0.9 for all combinations, except for combinations with channel y in System A in the first run, when it is slightly lower. The z-component of System B is very noisy in the late run, and it will be shown later on that this channel is not working properly at that time

In Figure 8 and Figure 9 the Fast Fourier Transform (FFT) spectra of the last and first data run can be compared. All FFT spectra shown here have been calculated using a Hamming window and after application of a detrend algorithm. The spectral content will be discussed in more detail in the next section, but the 16 2/3 Hz railway power frequency and the first Schumann resonance at 8 Hz are easy to recognize in the spectra. The largest differences between the beginning and the end of the data collection period are found in the vertical components, while the horizontal ones are more coherent.

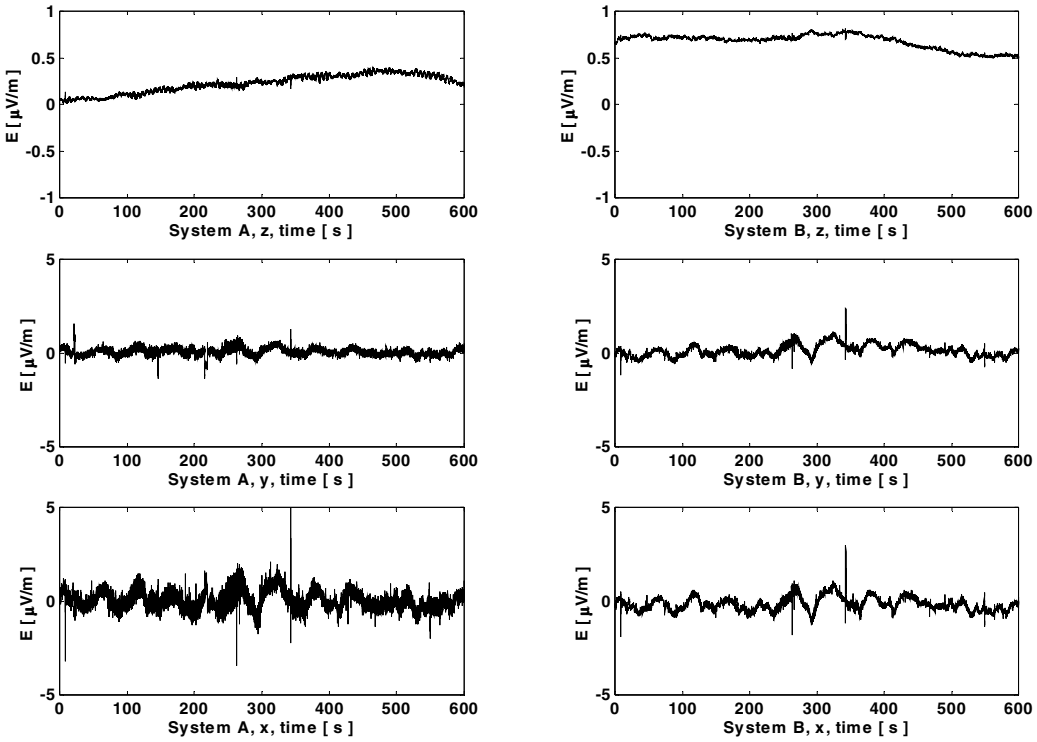

Figure 6: The time-series of the first data run used in the analysis, from 29 June 2000, 13:15.

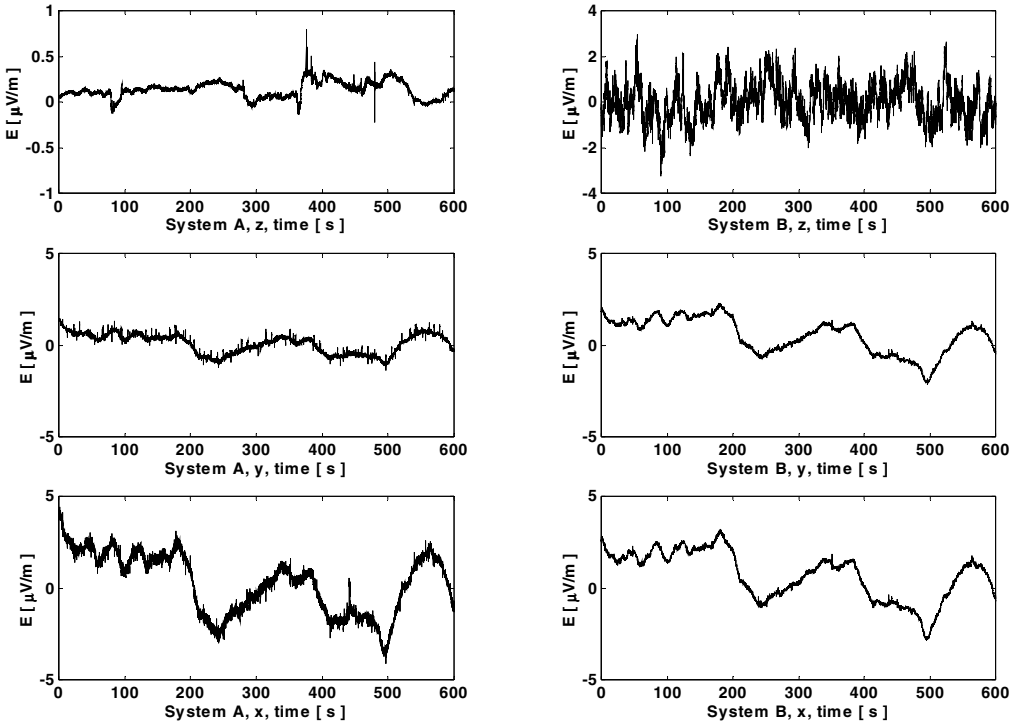

Figure 7: The time-series of the last run used in the analysis, from 29 April 2001, 00:15.

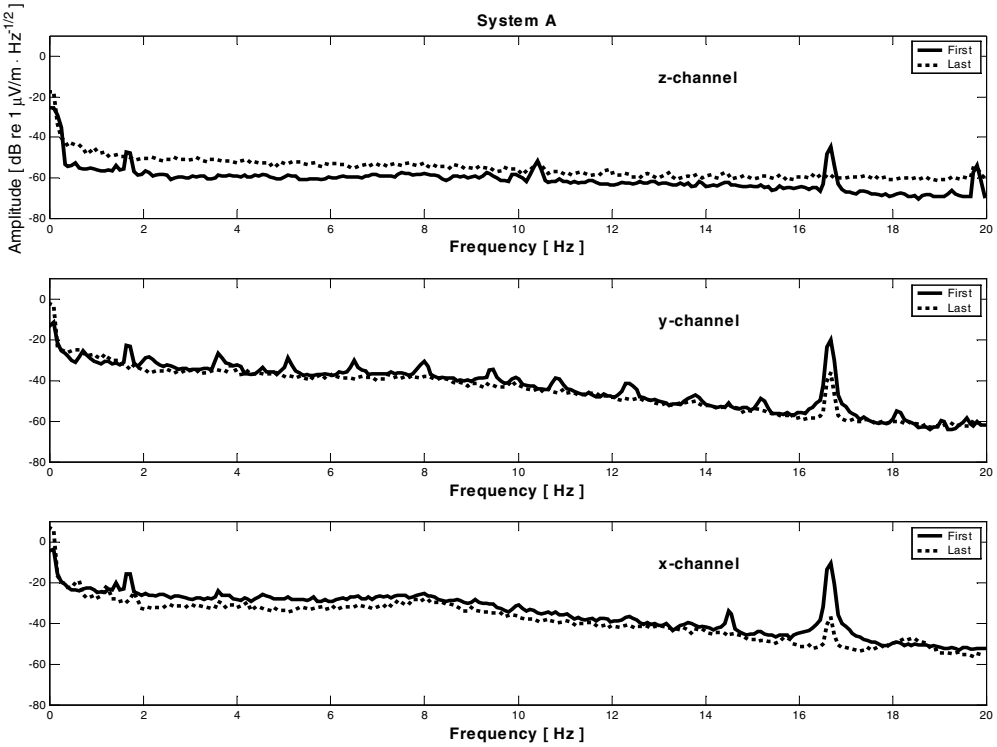

Figure 8: The FFT spectra of data from the first and the last analysed run, for System A. From top to bottom, the z, y, and x components are shown.

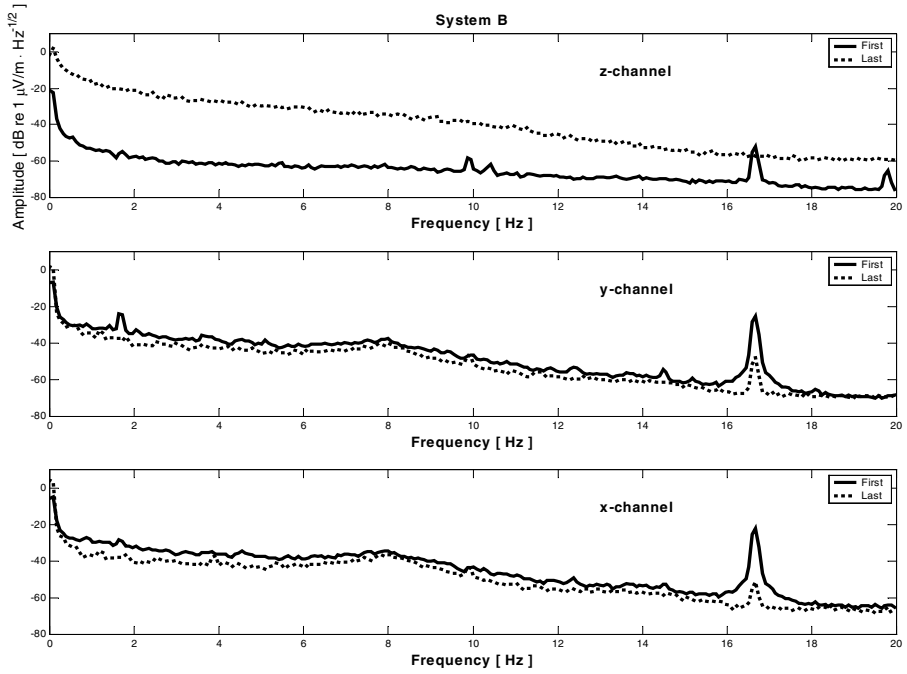

Figure 9: The FFT spectra of data from the first and the last analysed run, for System B.

A quick look through the whole data set reveals that the horizontal components of System B are the most reliable channels during the whole period. The y-component of System A has a few time-periods when there is a large low frequency (DC) component on top of the signal. The x-component of System A shows similar tendencies, but less pronounced and in shorter periods. Both vertical channels are working in the beginning of the period. They are sometimes dominated by noise. Since the geomagnetic fields are smaller in the vertical than in the horizontal direction, the signal to noise ratio is expected to be smaller for the vertical channels compared with the horizontal ones.

In an attempt to quantify the performance of the electrodes a number of parameters have been calculated and their evolution has been logged as a function of time. The methods used were, in short,

1. absence of a 'standard' signal, in this case the first Schumann resonance,
2. the stability of the mean value and standard deviation per run,
3. the correlation between each pair of equally aligned axes in the two systems.

More details about these methods are given in appendix 1-3.

The conclusion is that five of the six channels have survived the period and accordingly show a similar behaviour in the end as they did in the beginning of the measurements. One channel, the vertical channel of System B, fails towards the end of the period. Both vertical channels have periods when they are contaminated by electronic noise. As has already been pointed out, this might be expected, because the vertical fields are weaker than the horizontal ones. System A is in general noisier than System B. Apart from noise, System A has a period when there is a low frequency drift on top of its signals. Since only this system is affected it has to have a local origin within the electrodes themselves, in their electronics or in the near vicinity of System A.

It is hard to draw any firm conclusions whether the carbon fibre or silver-silver chloride electrodes perform better in the long run. The two systems are placed on different depths and in somewhat different environments. The conclusion must however be that all four horizontal electrode pairs are equally useful in the end of the trial as in the beginning 10 months earlier, and that only one electrode pair definitely has failed at the end.

4. The measured underwater electric field

4.1. Expected components of the field

The sources of the natural electromagnetic field can be grouped in the following way:

1. *Man-made sources*. Of particular importance here is the railway power at 16 2/3 Hz and harmonics of the power line frequency of 50 Hz and combinations of these two frequencies.
2. *Schumann resonances*. With their origin in thunderstorms around the world, the first resonance near 8 Hz and the second around 14 Hz are within the frequency range of the experiment.
3. *Micropulsations*. This is a common denominator for different events in the ionosphere or magnetosphere which generate fields from a few mHz to a few Hz. They are all ultimately driven by the solar wind.
4. *Tides and ocean currents*. When the ocean moves through the Earth's magnetic field, electromagnetic fields are induced in the water that can be large enough to be observable. No attempt has been made to identify any signals of this kind in this analysis.
5. *Special events*. A few examples of the effect on the underwater electric field when a ship passes above the sensor systems will be given.

Here, typical examples of sources 1-3 and 5 will be given.

4.2. Examples of underwater electric field signals

Railway power signal:

The 16 2/3 Hz signal due to the railway power is the strongest single component in the frequency spectrum. This conclusion can be drawn from Figure 10, which shows the dominating features of the data in the frequency domain. An FFT was calculated for each run and the figure shows the mean value over all runs. In this figure only signals with stable frequencies appear, while signals with time-dependent frequencies will be averaged out. Nor does temporary signals appear in this mean value. Since there are not many features at lower frequencies, a linear frequency scale has been chosen. The easiest identifiable features are the 16 2/3 Hz signal due to the railways, the 10 Hz aliased power-line signal and the first Schumann resonance, near 8 Hz. These sources belong to the first two types of expected sources listed in the previous section.

The 16 2/3 Hz signal is almost always present in the data. This is expected since there is a railway line in the harbour area. Thus, sources of this signal are located nearby the electrode systems. Strong transients are sometimes found; see Figure 11 and Figure 12. This type of event occurs rather frequently, in about one percent of the runs, and their amplitude can be large. They happen more often in the morning hours, in the 07:15 and 08:15 runs, and at noon. The amplitudes are often larger in System A than in System B.

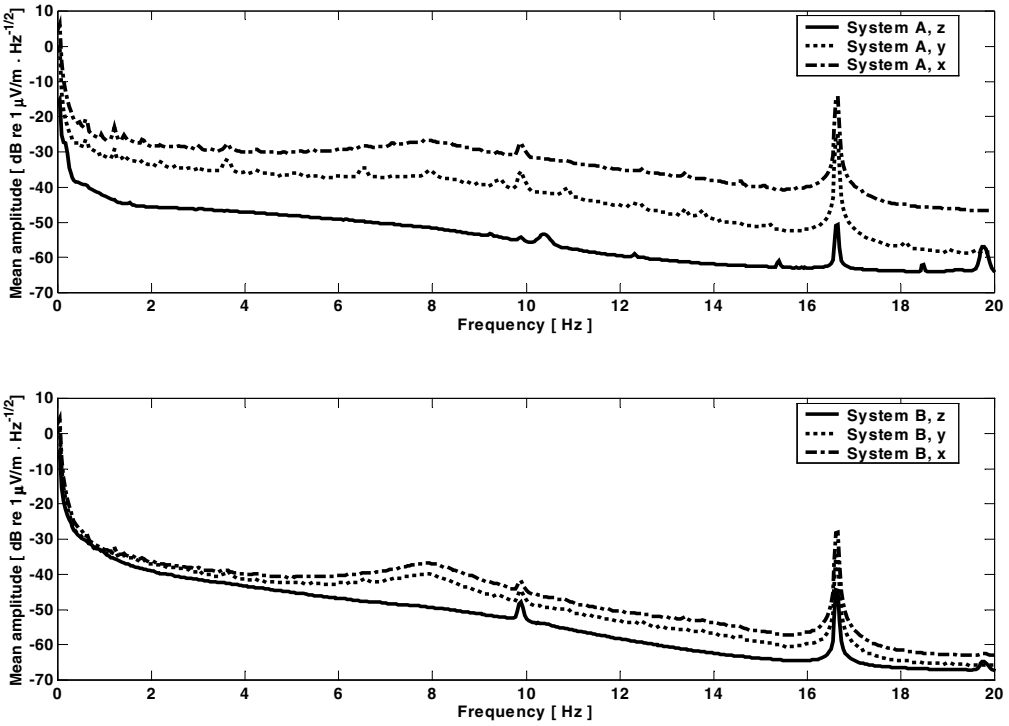

Figure 10: The mean value of all FFTs calculated for each of the analysed runs.

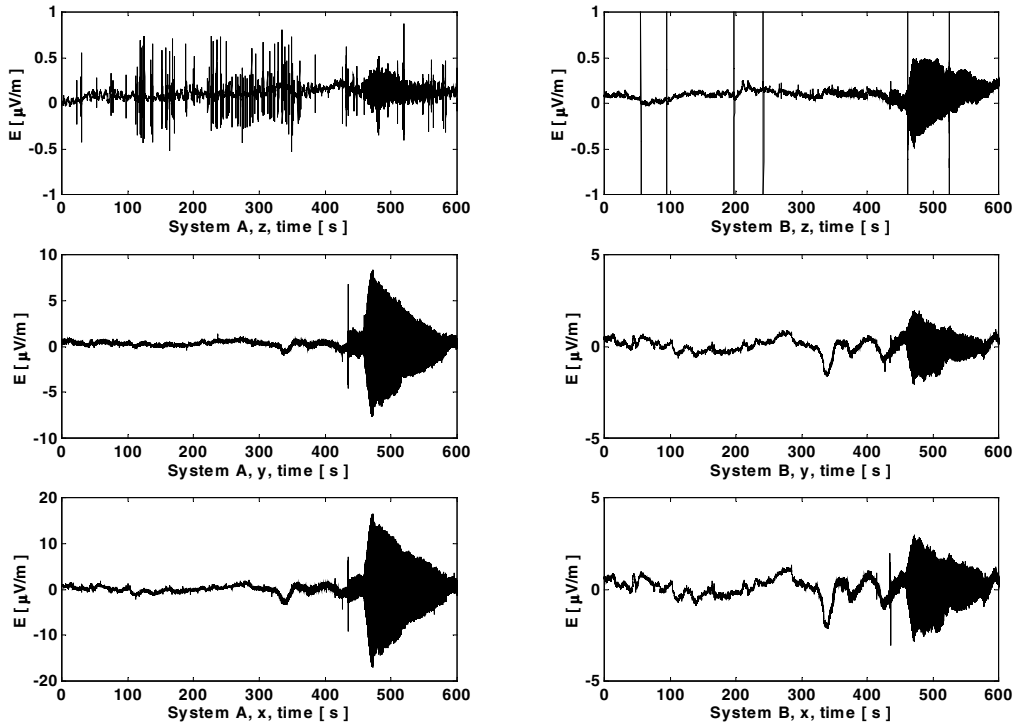

Figure 11: Sudden onset of the 16 2/3 Hz signal, at Monday morning, 13 November 2000, 07:15. Please note the varying y-scales of the different channels.

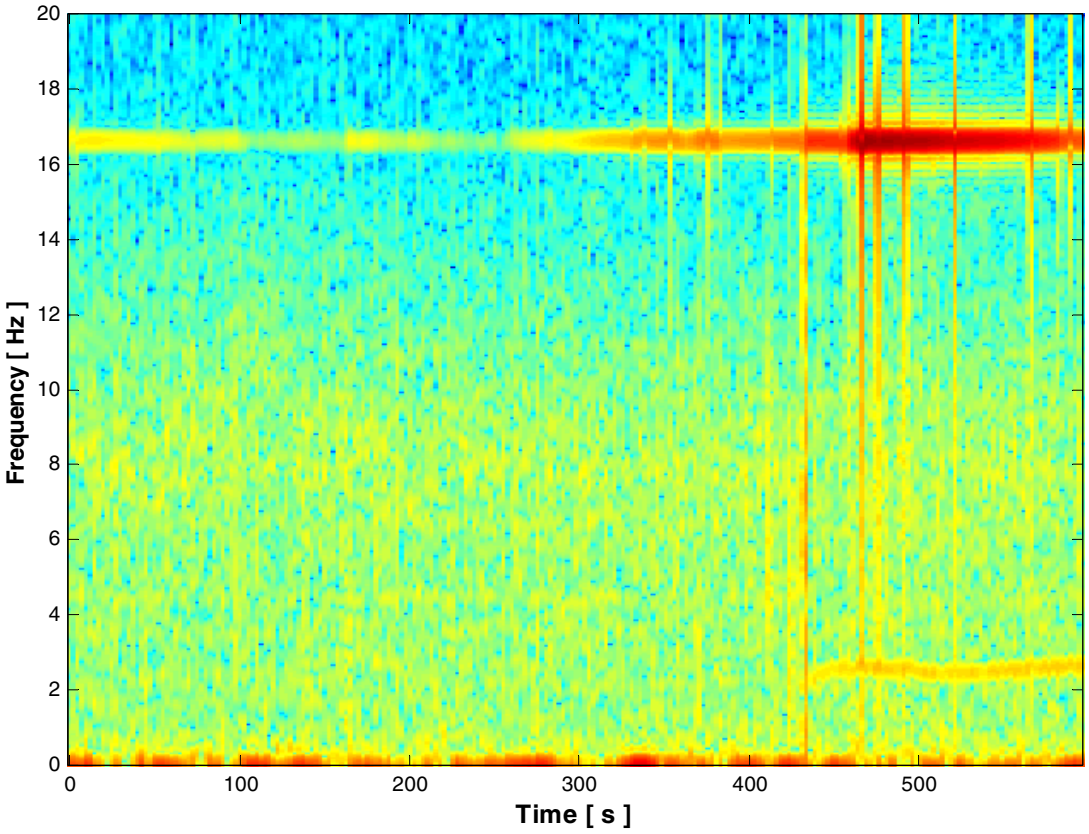

Figure 12: A time-frequency spectrogram which shows that the feature in the previous figure is due to the 16 2/3 Hz signal. This figure shows data from the x-component of System A, which has the largest amplitude.

50 Hz power

50 Hz is above the sampling frequency of 40 Hz and above the lowpass filter at 10 Hz. The filter is not steep enough to completely suppress the aliased frequency at 10 Hz (50 – 40 Hz). This is seen in Figure 10 where all channels have a peak near 10 Hz.

Schumann resonances

The first Schumann resonance was used for the long-term assessment of the performance of the data. The first two resonances, at about 8 Hz and 14 Hz [6] are within the frequency band covered by the measurements. The first resonance about 8 Hz is clearly seen Figure 10. The second harmonic is however difficult to identify in the data. This has many reasons; the amplitude is smaller than the first resonance and there is a low pass filter at 10 Hz. There is also the strong railway power signal that has a similar frequency. Schumann resonances are known to show variations in amplitude and peak frequency over time, both on long and short term [7-8]. Such amplitude variations are illustrated in Appendix 1, in Figure 23.

Micropulsations

Micropulsations are divided in Pc (continuous) and Pi (irregular) events. A commonly used classification scheme for micropulsations is shown in Table 2 [4]. Typical examples of events from the continuous micropulsation classes are given below, starting with the lowest frequencies.

Pulsation class	*f [Hz]*	*T [s]*
Pc 1	0.2-5	0.2-5
Pc 2	0.1-0.2	5-10
Pc 3	0.022-0.1	10-45
Pc 4	0.007-0.022	45-150
Pc 5	0.002-0.007	150-600
Pi 1	0.025-1	1-40
Pi 2	0.002-0.025	40-150

Table 2: Classification scheme for micropulsations.

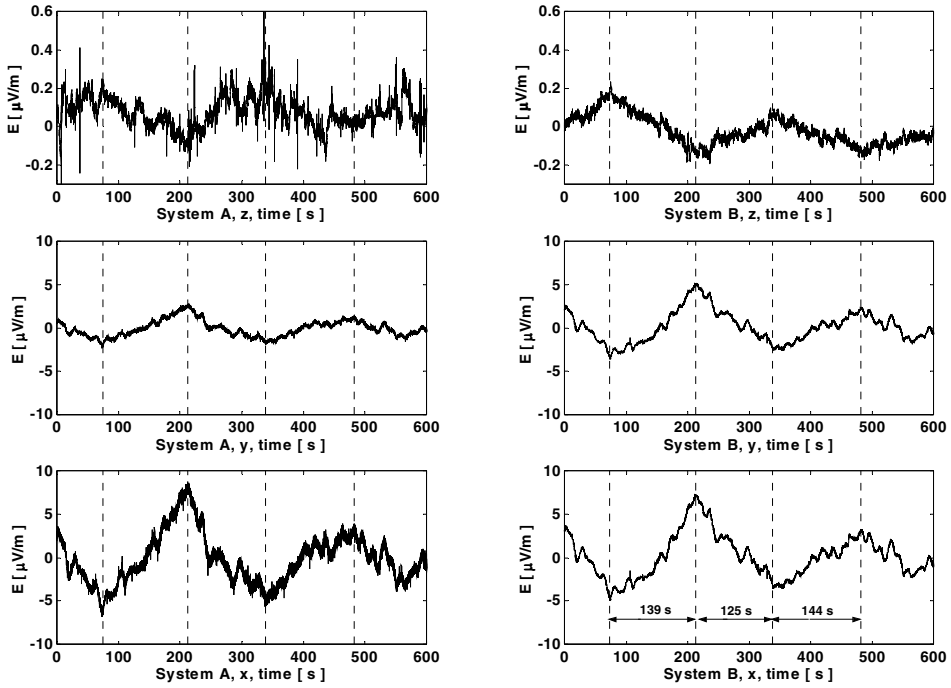

Figure 13: Pc 5 pulsations are expected with periods between 150-600 s. Here is an example with the approximate half-periods marked with the dotted lines. This event is from 10 November 2000.

i) Pc 5

The lowest frequency band that is possible to distinguish in the data is the Pc 5 band. It contains events with frequencies between 2 – 7 mHz, which means that they have periods between 150 – 600 s. With such long periods they are easily identified by looking in the time-domain of the data. An example is given in Figure 13. The period of the oscillations shown in that event is about 270 s.

ii) Pc 4

The next frequency band is between 7 – 22 mHz, or periods between 45 – 150 s. Again, this is slow enough to be seen by eye in the time-series, see Figure 14.

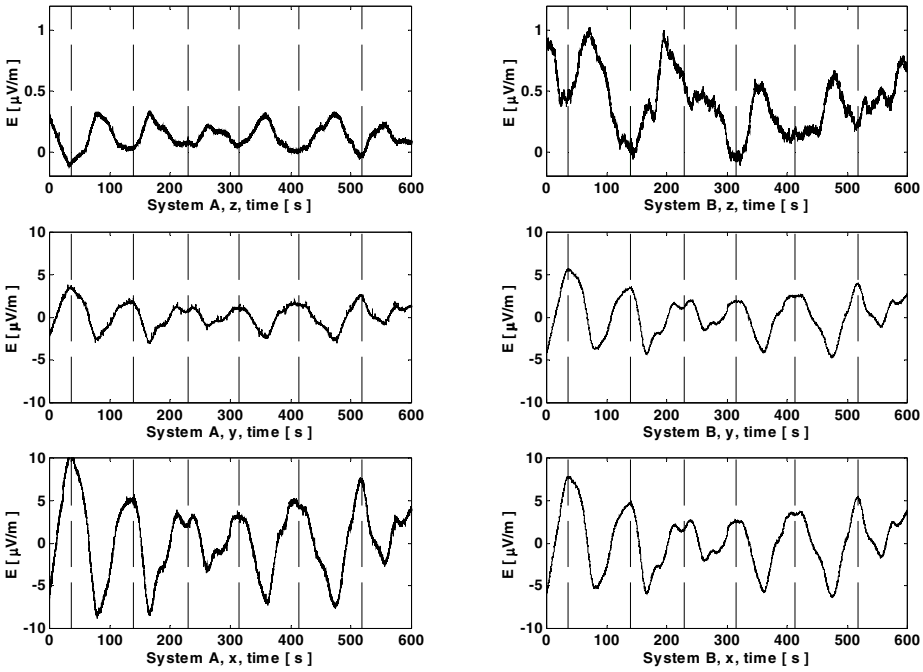

Figure 14: Data from 13 April 2001, 09:15. The dotted lines indicate the period of the oscillations, which varies between 86 s to 105 s.

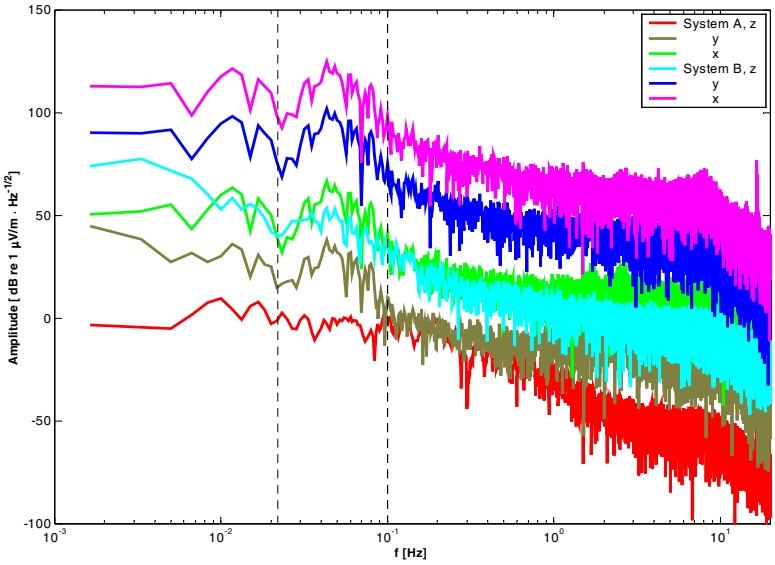

Figure 15: An example of a Pc 3 event in the frequency domain. This data is from 15 August 2000, 08:15. Please not that an offset of 20 dB has been added for each channel to make the figure more readable. The dotted lines show the limits of the Pc 3 frequency interval.

iii) Pc 3

This frequency band covers 22 – 100 mHz or periods between 10 – 45 s. A typical example is shown in the frequency domain in Figure 15.

To make the figure easier to read, an offset in steps of 20 dB has been added to the channels. Figure 16 shows the same data in the time-domain.

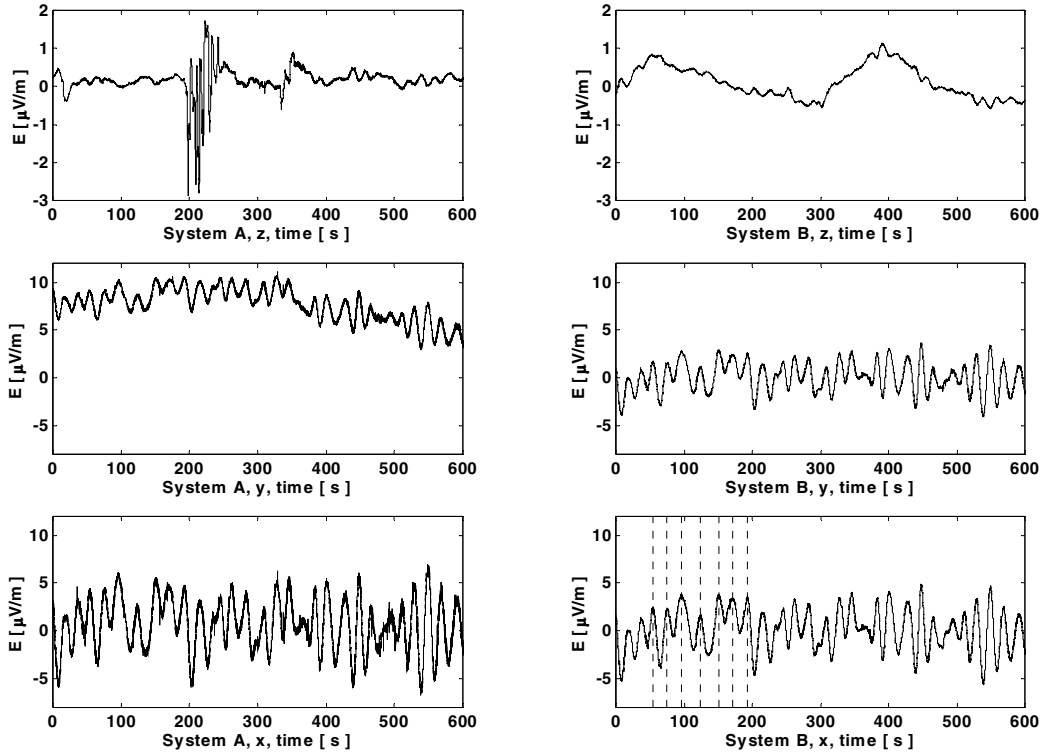

Figure 16: The same data as in Figure 15, shown in the time-domain. The periods of the oscillations which are marked with the dotted lines vary between 20 – 27 s.

v) Pc 1 and Pc 2

Pulsations with low frequencies are easily recognized in the time-domain, because the oscillations are slow enough on the time-scale of a complete 10-minute run. At higher frequencies, a shorter time-scale is needed for the pulsations to be clearly visible. Figure 17 shows a few minutes of a Pc 2 micropulsation.

These higher frequency events are also harder to recognize in the frequency domain. It is possible that the background is relatively higher at those frequencies. Another possibility is that these events are more rare than lower frequency pulsations. A solar maximum was reached in the summer of year 2000. An anti-correlation between the solar activity cycle and this type of events has been observed [5].

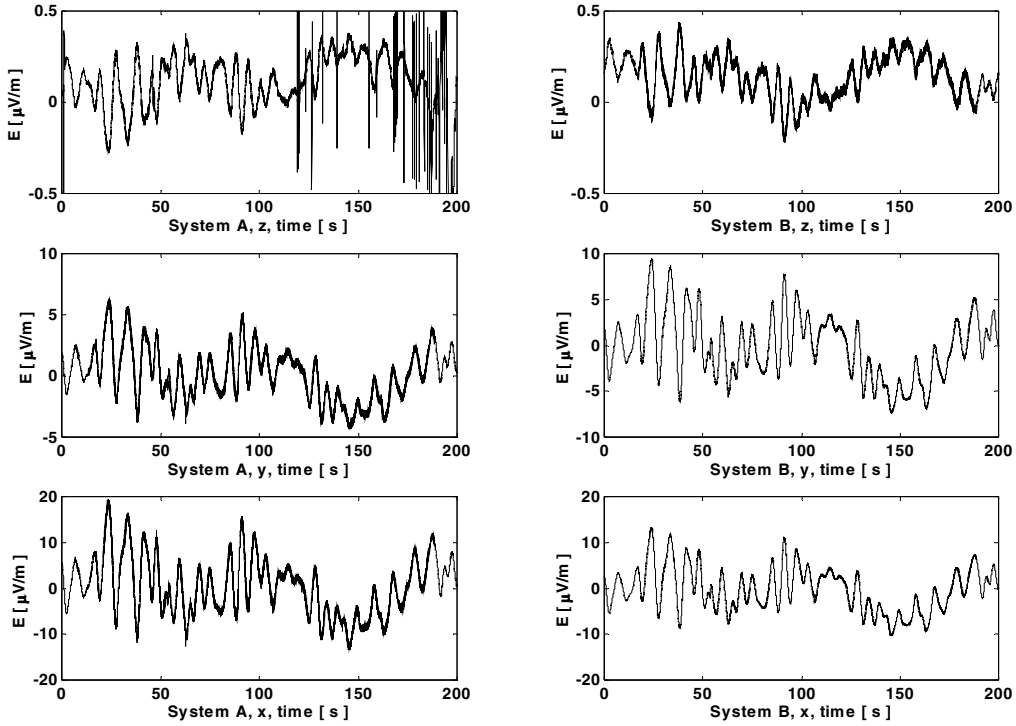

Figure 17: An example of a Pc 2 micropulsation. Note that the time-scale is different in this figure.

4.3. Special events

Some special events that probably are due to the passage of a ship above one of the systems have been identified. A very clear example of such a passage is shown in Figure 18. The distinct signature of a passage is seen with an amplitude that is much higher than the background at this time while there is no trace of this feature in the other system at this time.

Figure 19 shows another example, noteworthy of two reasons. Firstly, it shows that the vertical channel is not responding at this time, which is after the supposed failure at 19 April 2001. Secondly, the amplitude of the background was low at this time, which makes it possible to see the signal from the boat easily, although the maximum field induced by the boat was only 5 µV/m.

Both examples shown so far have been for System B. An example of a passage above the other System, System A, is shown in Figure 20.

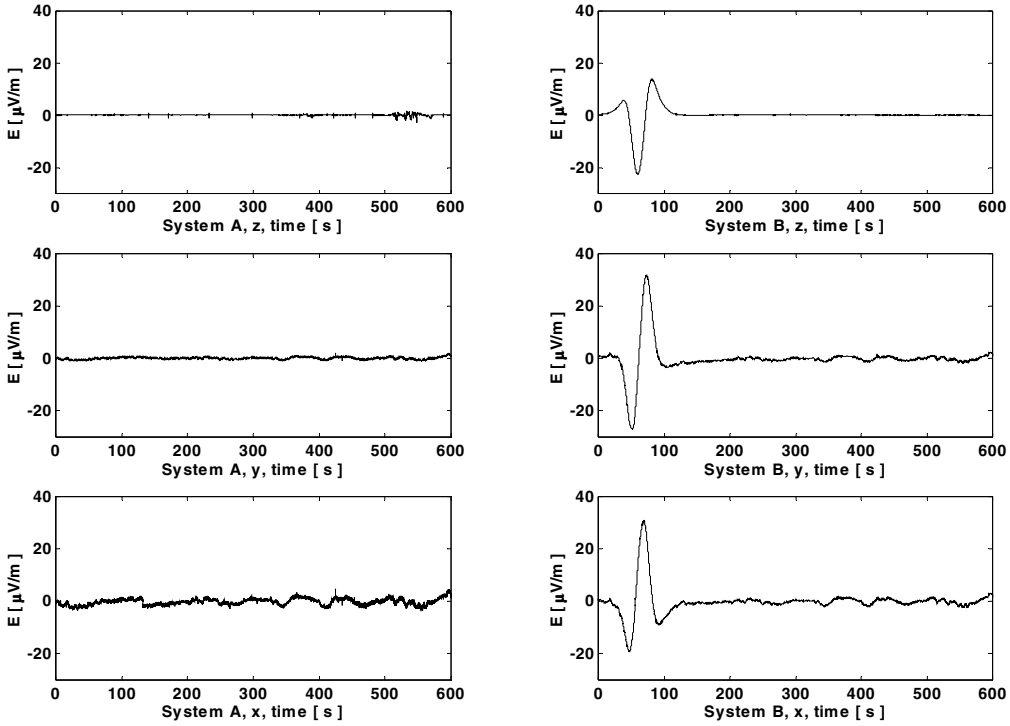

Figure 18: A very distinctive example of a passage of a boat above System B. This event happened on 11 November 2000.

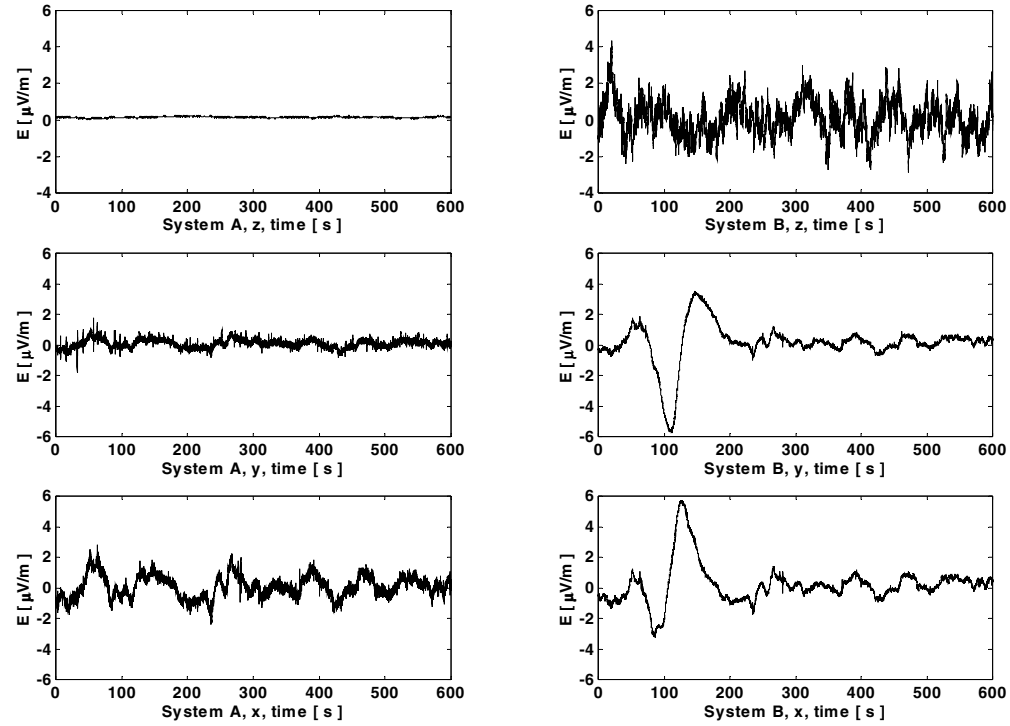

Figure 19 : An example of a boat passing nearby System B. Note that this data were collected after the failure of the vertical channel of that system. This data is from 25 April 2001.

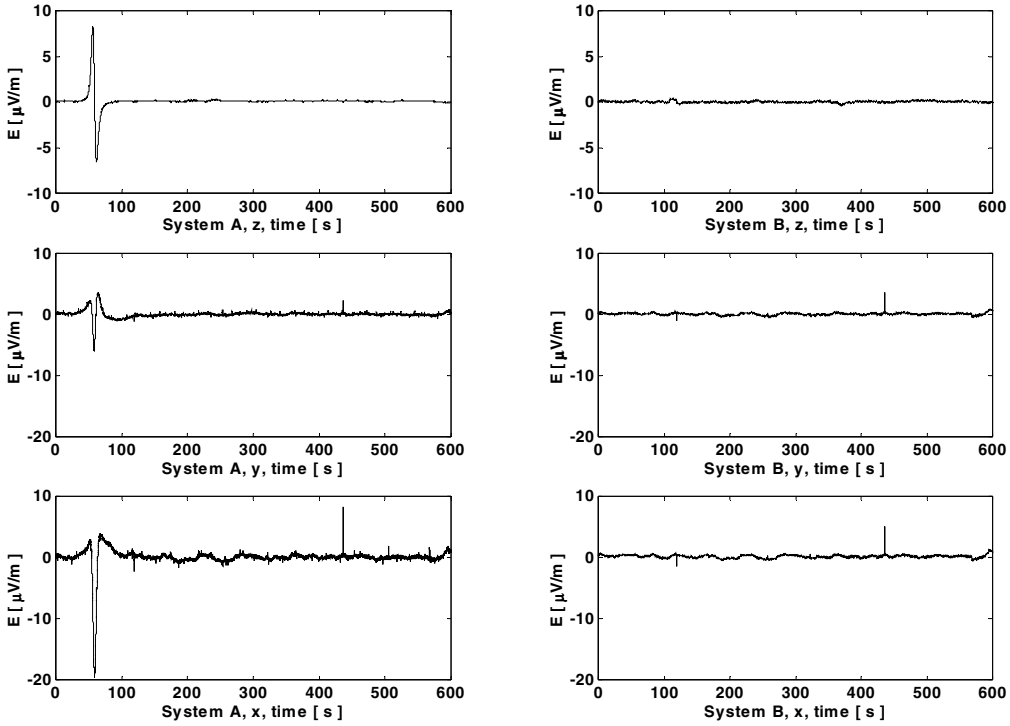

Figure 20: An example of a boat passing above System A.

5. Correlation between the systems

The correlation between the two systems has been investigated. Apart from occasions when there is some special event in the immediate vicinity of one of the systems (e.g. the passing of a ship) the correlation is expected to be high between System A and System B. This is because they are only separated by about 720 m, and a large part of the natural background has its origin in sources much further away. As a consequence any sudden change in the geomagnetic field can be considered to happen simultaneously in both systems. The cross-correlation for each run and between each pair of equally aligned axes of the systems has thus been calculated without taking into account any time-lag between the two systems. The result is shown in Figure 26 in appendix 3, where the long-term performance of the electrodes is studied with the correlation as a means. Apart from periods when the electrodes are unstable, the horizontal components have a high correlation over this relatively short distance.

In Figure 21 the correlation of the calculated total horizontal fields in the two systems is shown for data from a short time-period. The systems are not completely aligned, and correlation of the total horizontal field rather than the measurements from each axis separately is a way of avoiding any problems due to that. If Figure 21 is compared with Figure 26 the conclusion can be drawn that the correlation is indeed higher when the total horizontal field in the two systems is used.

In Figure 21 there is one run marked where the correlation between the two systems is particularly bad. The data from this run was shown earlier in Figure 18. The low correlation is explained by a local event above System B.

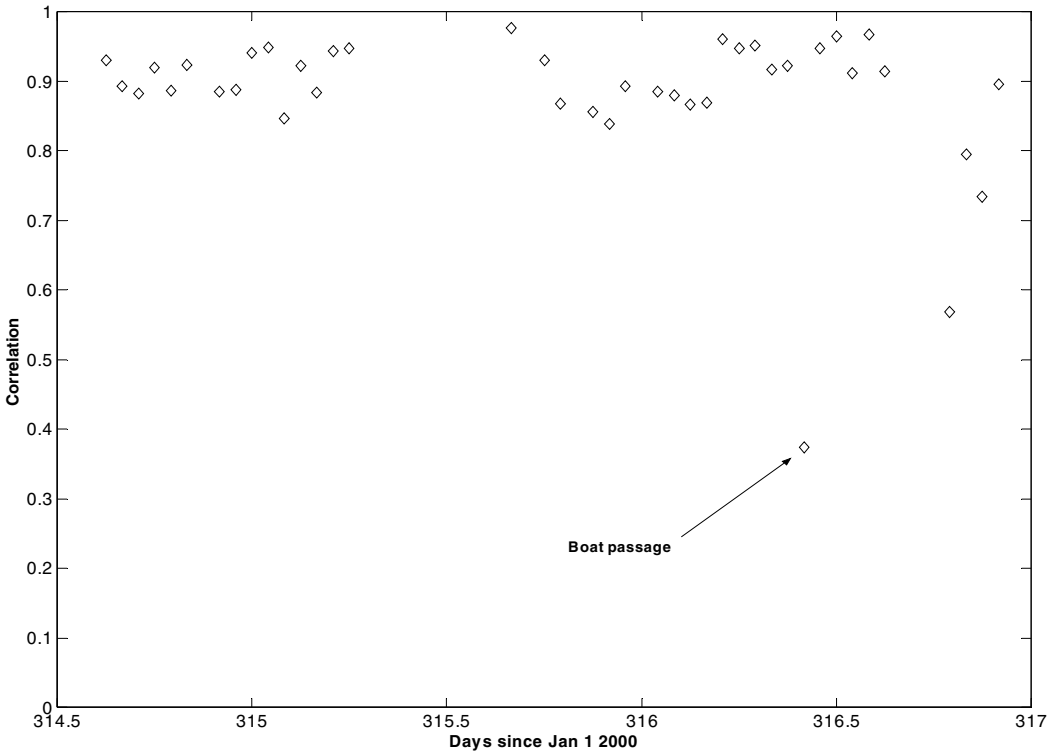

Figure 21: Correlation of the calculated total horizontal fields in both systems.

6. Conclusions

All four horizontal channels have survived the 10-month measurement. However, two of those, both belonging to System A (the silver-silver chloride electrode system) have time-periods when there is a large low-frequency component on top of the signal. One of them, which measure the smallest potentials, is also affected by high-frequency electronic noise from time to time.

One channel, the vertical channel of the carbon fibre System B, fails at the end of the measurement period. The vertical channels have in general less stable performance as a function of time than the horizontal ones.

The natural underwater electric field is due to sources of very different origins. Examples of the most important types of signals have been given. A more detailed study of the micropulsation signals and Schumann resonances and their amplitude and frequency variations over time is an interesting task for future research.

Further work should also be conducted concerning the correlation and also coherence of the signals at short and long range. The first results presented here show that the short-range (~ 700 m) correlation is high when the electrodes are functioning well, and there are no local events near one of the systems.

Appendix

1. Presence of a standard signal

One way to assess whether a reasonable signal is measured or whether the electrodes have failed is to look for the presence or absence of a 'standard' signal. Such a signal should ideally have a well-defined amplitude and frequency and be stable over time. In the absence of such an ideal signal we have tried to use the first Schumann resonance. Unfortunately none of the criteria above are fulfilled, and it is only possible to try and assess the presence of a Schumann-like signal in the frequency spectra. Schumann resonances are caused by lightning activity on a global scale, which excite the Earth-ionosphere spherical cavity [6]. The first resonance is found just below 8 Hz and the second around 14 Hz. Their peak frequencies varies on time scales from days to years [7].

Here a window between $f_1 = 6.5$ Hz and $f_2 = 9.5$ Hz was used. To get an estimate of the signal at those frequencies in the absence of the Schumann resonance, the following model was used:

$$A(f) = \frac{A(f_2) - A(f_1)}{f_2 - f_1}(f - f_1) + A(f_1)$$

where $A(f)$ is the FFT amplitude. The summed difference between data, $X(f)$, and this model was calculated as

$$D = \sum_{f=f_1}^{f_2} (A(f) - X(f))$$

The result is shown in Figure 22, where the largest features appear in the vertical channels. The vertical component in System A has a

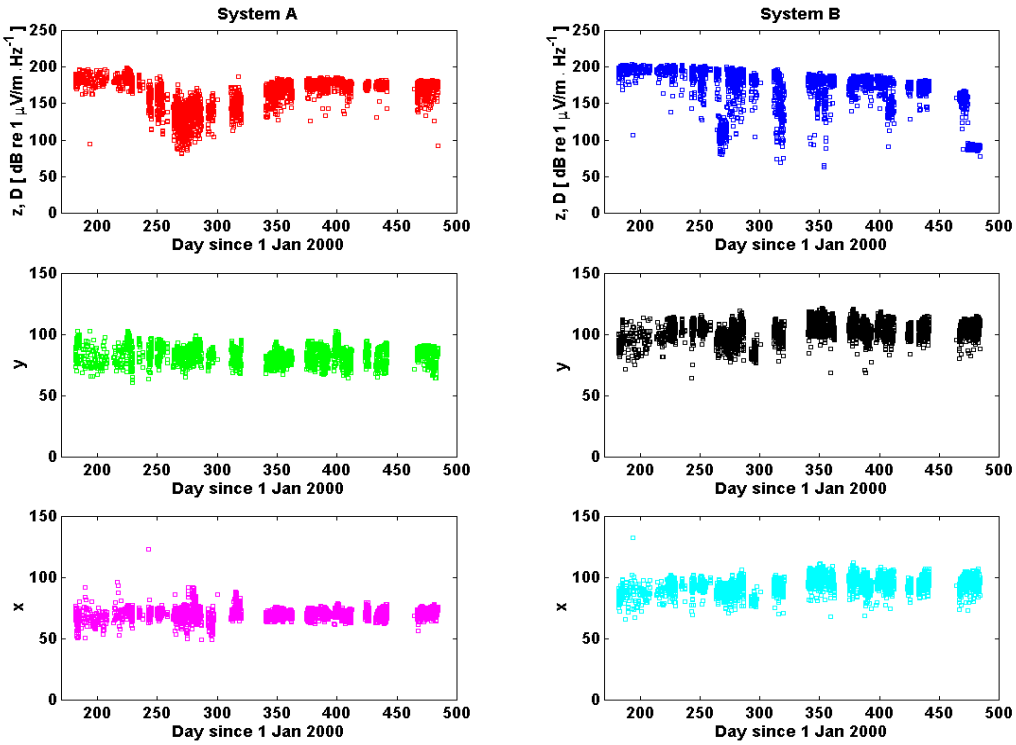

Figure 22: The summed difference in amplitude between data and the model in the frequency interval 6.5-9.5 Hz, centred on the first Schumann resonance.

period where the amplitude is lower. A closer look at the signal at those times reveals that the signal is very noisy, so that any signal due to the Schumann resonance will be difficult to extract. The other vertical channel is also very noisy.

All channels have a pronounced spread in their amplitudes. One explanation is illustrated in Figure 23. When viewed at the shorter time-scale of that figure, a pattern is revealed with daily variations in the amplitudes. This is an example of the daily variations in the Schumann resonances that are known from other measurements [7]. The measured signal at a remote site depends on the distance between the measurement site and the area where the lightning takes place, and this area will move on a daily basis [8].

There is a sudden decrease in the amplitude of the z-component of System B at the end of the measurement period, see Figure 22. It is due to a sudden increase in the higher frequency noise between two runs on 19 April 2001. After this time, noise is completely dominating this channel, and the time-series looks like the one shown earlier in Figure 7. This sudden change in behaviour is shown in Figure 24. It shows FFT versus time for 8 consecutive data runs. The change appears between the data collected at 14:15 and 15:15 on this day, and the channel is obviously not working after this time.

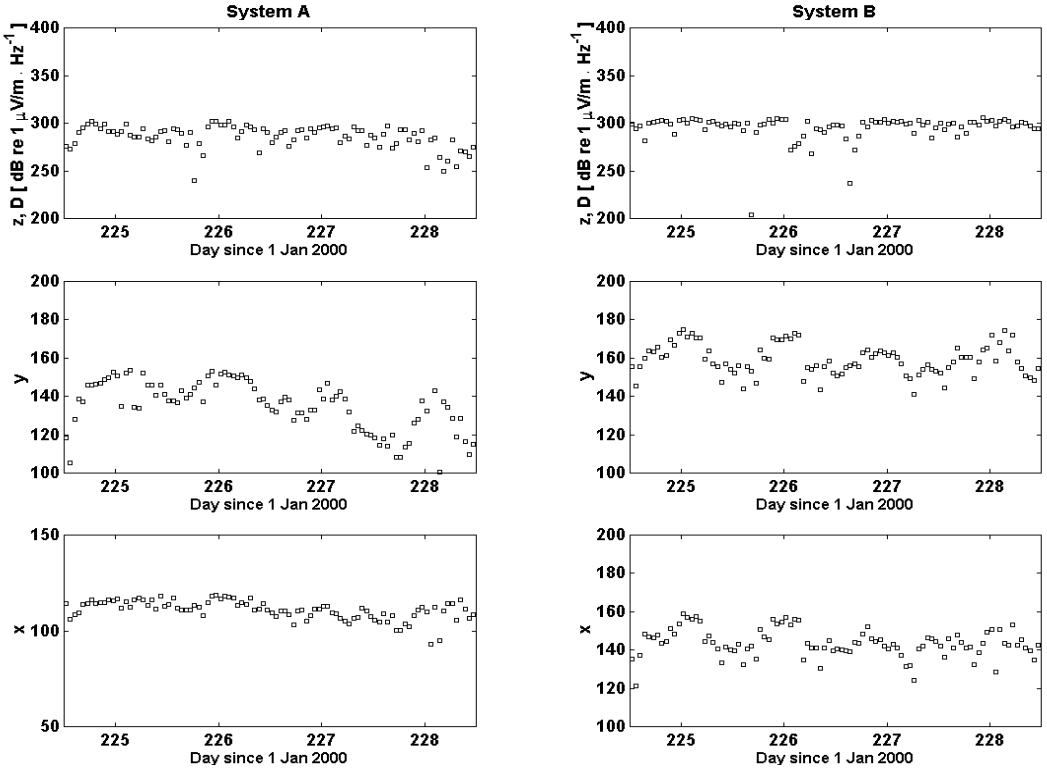

Figure 23: Example of daily variations in the amplitude of the first Schumann resonance.

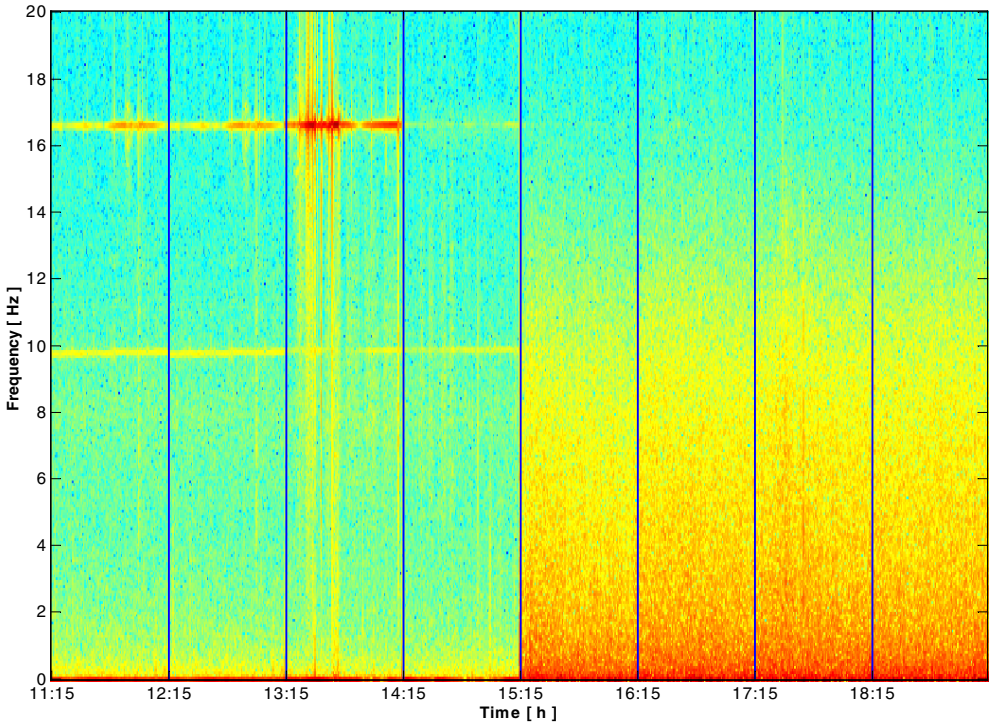

Figure 24: FFT spectrum versus time for the vertical channel of System B during 19 April 2001. The data from 8 consecutive 10-minute acquisitions is shown one after the other. A blue line separates each run, and it is 50 minutes between each run.

2. Mean value and standard deviation

When the electrodes are working properly, the mean value and standard deviation calculated over 10 minute intervals should be constant over time. The mean value and standard deviation was calculated for each run. The mean, μ_i, and standard deviation, σ_i, for each individual run i was combined in a common mean per week

$$\hat{\mu} = \frac{1}{w}\sum_{i=1}^{N} w_i \mu_i$$

where μ_i is mean of each run and the weights, w_i, are

$$w_i = \frac{1}{\sigma_i^2}$$

and w is the sum of all w_i.

Figure 25 shows the result. The most striking features in Figure 25 are found for the horizontal electrode pairs in System A. Not only are the mean values higher than average around weeks 30 – 40, the standard deviations are larger as well. At this time there is a very low frequency component in the signals, which causes the mean-values to be large. However, the higher frequencies are not affected, and the FFT spectra are almost identical to the ones calculated for the horizontal components of

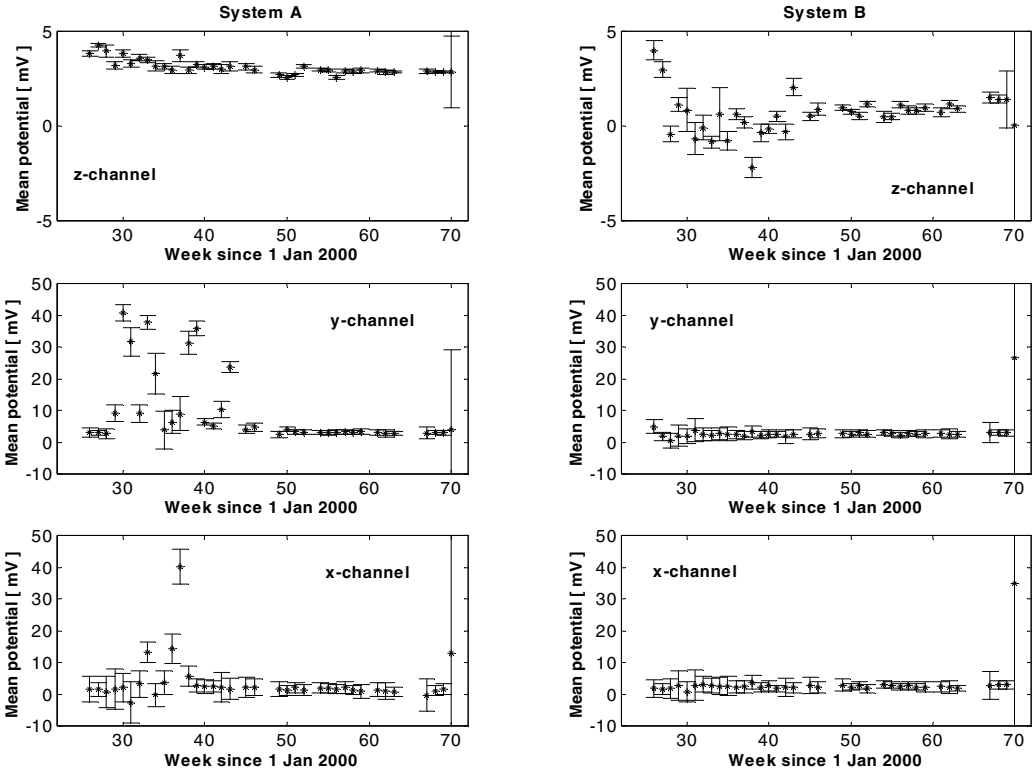

Figure 25: The time-evolution of the mean values and standard deviation calculated per week.

System B. The reason why this happens is unknown. Since it affects both horizontal channels in System A, but not the ones in System B, the reason has to have a local origin within the electrodes themselves, in their electronics or in the near vicinity of System A in the water.

The error bar of the last week, week 70, is unusually large. This is because it is based on one run only, since the last data run was at Sunday 29 April 2001 at 00:15. The weeks are numbered from 1 January 2000, which was a Saturday; all weeks start with a Sunday. All the other values are based on a much larger number of runs, which was shown in Figure 4.

3. Correlation between the two systems

There are two systems available with almost equal orientation in the geomagnetic field and at relatively short distance from each other. It is thus expected that they should have well correlated signals. In case one pair of electrodes fails, this correlation should decrease. A long-term logging of the correlation can thus be a tool for finding out if a pair of electrodes suddenly stops operating correctly.

The cross-correlation has been calculated for each sensor axis with equal orientation and the result is shown in Figure 26. The vertical axes have low correlation. The horizontal axes have higher correlation, except for one time-period. This period coincides with the one where the mean values for the horizontal channels of System A were larger than normal, explained by the anomalous low frequency component in those signals. The correlation is better between the x- than the y-components. The reason might be in the y component of System A. This channel measures smaller potentials in general than the other channels, and might be more affected by electronic noise.

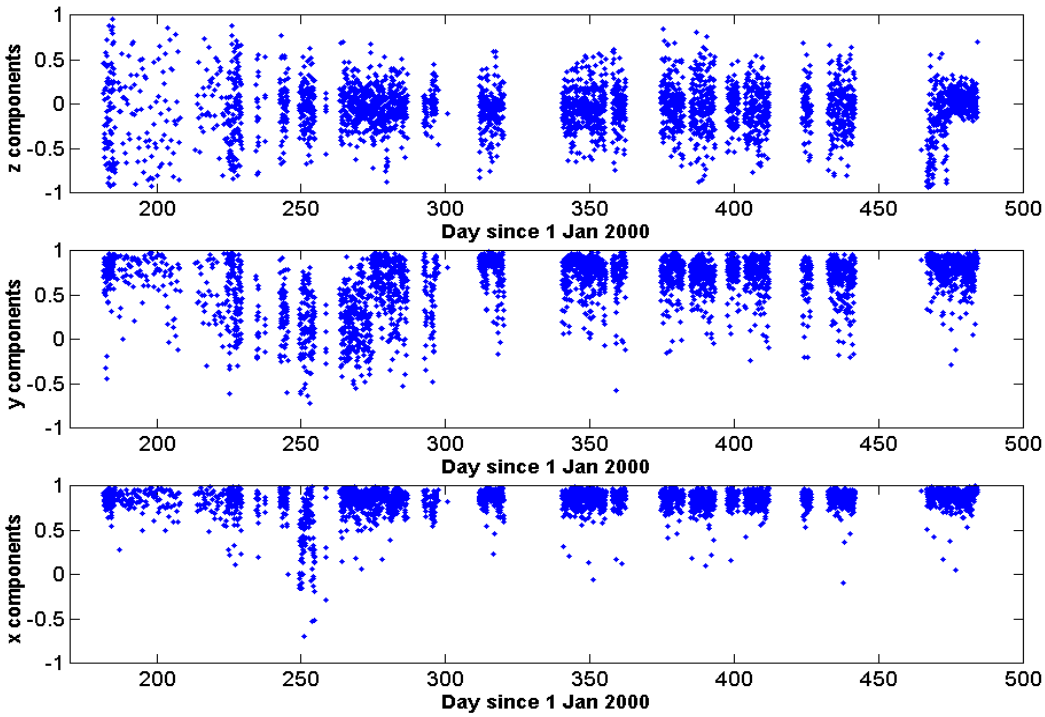

Figure 26: Cross-correlation between System A and System B.

The correlation between the vertical channels decreases drastically at day 473. In Appendix 1, where the presence of the first Schumann resonance was investigated, it was found that this channel fails at this time.

It should be stressed that a single value of low correlation does not mean that one of the channels is broken. Instead this could indicate a local event near one of the electrode pairs. It is the long-term behaviour that can be used as a diagnostic tool for performance evaluation.

References

[1] Filloux, J.H., *Instrumentation and Experimental Methods for Oceanic Studies*, in *Geomagnetism*, Jacobs, J.A. (ed.), Academic Press (1987)

[2] Brage, A., *Electrochemical Characterisation of Carbon Fibre Electrodes for Underwater ElectricPotential Measurements,* 2nd International Conference on Marine Electronics, MARELEC, 1999

[3] Nygren, H.-G, *Lågbrusig galvaniskt isolerad förstärkare för lågresistiva sensorer*, FOA-R-94-00073-2.2-SE, 1994

[4] Campbell, W.H., *Introduction to Geomagnetic Fields*, Cambridge University Press (1997)

[5] Trakhtengerts, V.Y., Demekhov, A.G., Belyaev, P.P., Polyakov, S.V., Ermakova, E.N., & Isaev, S.V., *A mechanism of anticorrrelation in the occurrence of ULF electromagnetic noise resonance structure and Pc 1 magnetic pulsations through the solar activity cycle,* Journal of Atmospheric and Solar-Terrestrial Physics 62, 253-256 (2000)

[6] Barr, R., Llanwyn Jones, D., & Rodger, C.J., *ELF and VLF radio waves,* Journal of Atmospheric and Solar Terrestrial Physics **62,** 1689-1718 (2000)

[7] Sátori, G., *Monitoring Schumann resonances – II.Daily and seasonal frequency variations,* Journal of Atmospheric and Solar Terrestrial Physics **58,** 1483-1488 (1996)

[8] Nickolaenko, A.P., Sátori, G., Zieger, B., Rabinowicz, L.M., & Kudintseva, I.G., *Parameters of global thunderstorm activity deduced from the longterm Schumann resonance records*, Journal of Atmospheric and Solar-Terrestrial Physics **60**, 387-399 (1998)